

Surface Acoustic Load Sensing Using a Face-Shear PIN–PMN–PT Single-Crystal Resonator

Kyungrim Kim, Shujun Zhang, and Xiaoning Jiang

Abstract— $\text{Pb}(\text{In}_{0.5}\text{Nb}_{0.5})\text{O}_3\text{-Pb}(\text{Mg}_{1/3}\text{Nb}_{2/3})\text{O}_3\text{-PbTiO}_3$ (PIN–PMN–PT) resonators for surface acoustic load sensing are presented in this paper. Different acoustic loads are applied to thickness mode, thickness-shear mode, and face-shear mode resonators, and the electrical impedances at resonance and anti-resonance frequencies are recorded. More than one order of magnitude higher sensitivity (ratio of electrical impedance change to surface acoustic impedance change) at the resonance is achieved for the face-shear-mode resonator compared with other resonators with the same dimensions. The Krimholtz, Leedom, and Matthaei (KLM) model is used to verify the surface acoustic loading effect on the electrical impedance spectrum of face-shear PIN–PMN–PT single-crystal resonators. The demonstrated high sensitivity of face-shear mode resonators to surface loads is promising for a broad range of applications, including artificial skin, biological and chemical sensors, touch screens, and other touch-based sensors.

I. INTRODUCTION

PIEZOELECTRIC resonators are widely used in applications in the chemical, bio-medical, semiconductor, and information industries because of their merits of simple structure and low cost. For example, microbalances which are made of quartz or other piezoelectric material can be used for sensing the degradation of fuel cells by measuring the corrosion on the surface area of electrodes [1]. They also have been used as highly sensitive humidity sensors because the microbalances are very stable devices, and thus, can detect small mass changes (less than a nanogram) of vapor deposition [2]. In the medical field, piezoelectric tactile sensors have been developed for measuring the elastic stiffness of tissues [3]–[6], for the endoscopic sensor in minimally invasive surgery (MIS) [7], [8], for the smart skin used in diagnosing breast tumors or prostate gland disease [9], and also for sensing the intraocular pressure (IOP) in the human eye [10]. Information-industry applications include touch input devices, fingerprint identification, and virtual reality video game devices [11]. Typically, these types of sensors use direct piezoelectric effect or measure changes in the resonant frequency of oscillation

caused by interaction between piezoelectric resonator arrays and target materials. The change in the resonant frequency is directly proportional to the applied force by the Sauerbrey equation [12]. Thus, the local distribution of the applied mechanical stress can be detected by measuring the fundamental frequency shift of the resonator array. However, to obtain the tactile information from the object, the time duration of applied stress must exceed the required time for array scanning and data processing. In this case, the parallel scanning process can be used to speed up the scanning of the sensor array [13]. A relatively new tactile sensing technique, which uses the relationship between electrical impedance of the piezoelectric resonator and acoustic load impedance of the front load, has been developed for the fingerprinting application [14], [15]. The sensing component was made of a piezoelectric composite [lead zirconate titanate (PZT)/epoxy 1–3 composite] with diced electrodes forming a 2-D array. When an object is applied to the front surface of sensor, the electrical impedance of piezoelectric elements at a particular frequency is changed. This change is related to the acoustic impedance of applied objects. As a result, the distribution of acoustic load impedance of the object can be mapped by measuring the electrical impedance of each element of the array in a rapid fashion. This device can be highly sensitive as a biometric sensor compared with capacitive and thermal tactile sensors because the contrast ratio of acoustic impedance between air and tissue is 4000:1, whereas that of thermal conductivity is about 8:1 and dielectric permittivity is 32:1 [16]. For these reasons, this acoustic impedance sensing is promising for applications in biomedical industry (artificial skin sensor) and service robotics (touch screen and fingerprint reader).

The PZT ceramics are commonly used piezoelectric materials for the aforementioned sensors because of their high dielectric constants, large electromechanical coupling factors, and ease of manufacturing [17]. Lead magnesium niobate–lead titanate (PMN–PT) single crystals have also been investigated as promising candidates with advanced properties compared with PZT [18], [19]. For example, the elastic compliance of PMN–PT is about 6 times higher than that of PZT–5H. A high elastic compliance leads to reduced element and device size for a given resonance frequency. The piezoelectric coefficient of PMN–PT is 3 to 5 times higher than that of PZT–5H, which determines the performance of the piezoelectric device. In addition, PMN–PT has a higher electromechanical coupling factor (longitudinal mode, k_{33}): greater than 0.90 compared

Manuscript received March 15, 2012; accepted August 8, 2012. The work is partially supported by the North Carolina State Career Development Fund provided to X. Jiang.

K. Kim and X. Jiang are with the Department of Mechanical and Aerospace Engineering, North Carolina State University, Raleigh, NC (e-mail: xjiang5@ncsu.edu).

S. Zhang is with Materials Research Institute, The Pennsylvania State University, University Park, PA.

DOI <http://dx.doi.org/10.1109/TUFFC.2012.2488>

TABLE I. MEASURED PROPERTIES OF THE CRYSTAL.

	f_r (kHz)	f_a (kHz)	$\epsilon_{33}^T/\epsilon_0$	s_{66}^E (m ² /N)	k_{36}	d_{36} (pC/N)	N_{36} (Hz·m)
Values	68.25	93.45	2940	111×10^{-12}	0.76	1280	682

with 0.75 of PZT-5H [20], [21]. A much broader operating bandwidth can be achieved with a large coupling factor [18], [22]. For these reasons, PMN-PT crystals have been used in various devices such as sensors, actuators, and other electromechanical devices in advanced medical applications [18]. However, the low coercive field (2.5 kV/cm) of binary PMN-PT crystal can limit its application, which requires a high excitation signal [18], [23]. Furthermore, the low depoling temperature ($T_{R/T} = 75^\circ\text{C}$ to 95°C) can be a cause for reduced performance of the devices [24]. Recently developed ternary PIN-PMN-PT crystals retain similar electromechanical couplings ($k_{33} > 0.9$) and piezoelectric coefficients ($d_{33} > 1500$ pC/N) compared with the binary PMN-PT, but have significantly improved coercive field (5 kV/cm), and $T_{R/T}$ (117°C) [18], [25], [26]. In the case of the thickness-shear mode, the high shear piezoelectric coefficients (d_{15}) and electromechanical coupling factors (k_{15}) for different domain configurations were also observed to be >2000 pC/N and >0.85 , respectively [27]. More recently, the face-shear mode PIN-PMN-PT crystals have been given attention because of their ultra-low frequency constant (500 Hz·m) and high piezoelectric coefficient (2000 to 2500 pC/N) [28]. The low frequency constant allows the piezoelectric device to be small for ultra-low-frequency applications such as sonar transducers. More importantly, unlike thickness-shear-mode crystals, the face-shear-mode crystals can be easily repolarized because the poling electrode is the same as the active electrode. Moreover, the face-shear-mode PIN-PMN-PT crystals have significantly higher mechanical quality factor Q_m (150 to 180) than that of thickness-shear crystal (20 to 30) [18], [28], which is promising in resonator applications.

In this paper, the face-shear-mode PIN-PMN-PT single-crystal resonators were first fabricated and characterized by measuring properties such as shear piezoelectric

coefficients (d_{36}), electromechanical coupling factors (k_{36}), elastic compliance (s_{66}), and frequency constant (N_{36}) using the resonance method. Different acoustic loads were then applied to the thickness-mode, thickness-shear-mode, and face-shear-mode crystal resonators to compare the sensitivity to electrical impedance change induced by the applied acoustic loads. The experimental results were verified by a Krimholtz, Leedom, and Matthaei (KLM) model simulation.

II. FACE-SHEAR PIN-PMN-PT SINGLE CRYSTAL

In this study, [011]-cut rhombohedral PIN-PMN-PT single crystals were used, which have the macroscopic symmetry mm2. The crystals were oriented using a real-time back-reflection Laue system. Face-shear-mode samples were prepared by rotating a 45° angle about the Z-axis [011] direction, with dimensions of $10 \times 10 \times 1$ mm. Electrodes were deposited on the (011) surface of each crystal. The samples were poled along the crystallographic [011] direction. The capacitance of the face-shear PIN-PMN-PT single crystal was measured at 1 kHz and the free dielectric constant ($\epsilon_{33}^T/\epsilon_0$) was found to be 2940. The resonant frequency (f_r) and anti-resonant frequency (f_a) were also measured using an impedance analyzer (HP4294A, Agilent Technologies Inc., Santa Clara, CA) and found to be 68.25 and 93.45 kHz, respectively. Properties of the crystals can be calculated according to the IRE standards [29], [30]. Table I shows the measured and calculated properties of the face-shear PIN-PMN-PT single crystal. Compared to the published data [30], the overall properties showed slightly lower values. This might be attributed to the fact that the sample properties are related to the crystal composition of the sample used.

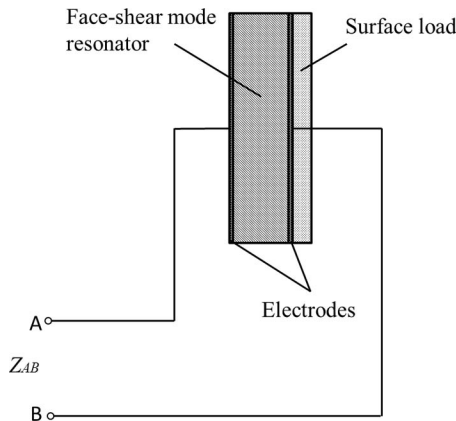


Fig. 1. The schematic of the single-surface loaded piezoelectric face-shear-mode resonator.

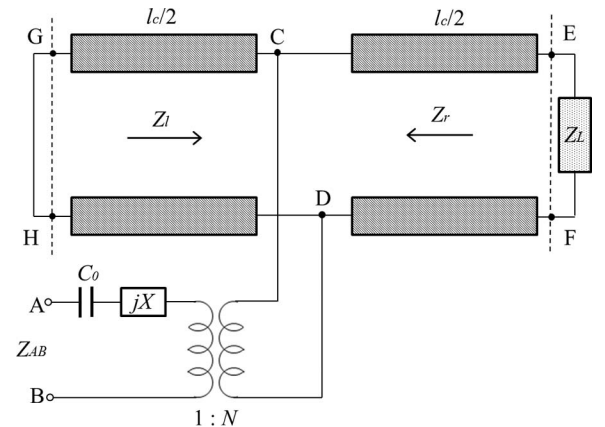


Fig. 2. The equivalent circuit for a single-side loaded piezoelectric crystal using the Krimholtz, Leedom, and Matthaei (KLM) model.

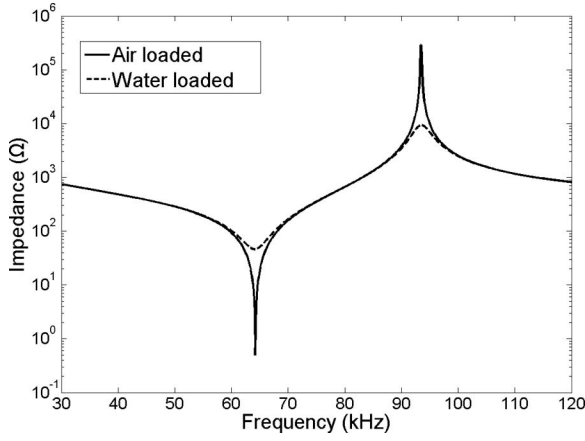


Fig. 3. Electrical impedance spectrum of the face-shear-mode resonator with the front load.

III. SURFACE LOAD SENSING MODEL

Fig. 1 indicates the schematic of the single surface loaded piezoelectric face-shear mode resonator. The surface load can be any material, including air, water, metal, and rubber. Z_{AB} represents the electrical impedance of piezoelectric resonator. The acoustic impedance changes from the surface load of the resonator can be sensed by measuring the change of the electrical impedance (Z_{AB}). The KLM model [31] was used to verify the effect of the acoustic loading on the face-shear-mode PIN-PMN-PT crystal. Fig. 2 represents the equivalent circuit of the KLM model [32]. The acoustic impedance at the port CD is a combination of the right acoustic impedance (Z_r) and the left acoustic impedance (Z_l). Z_r and Z_l are given by [33]

$$Z_r = Z_c \frac{Z_{EF} + Z_c \tanh(\gamma_c l_c/2)}{Z_c + Z_{EF} \tanh(\gamma_c l_c/2)} \quad (1)$$

$$Z_l = Z_c \frac{Z_{GH} + Z_c \tanh(\gamma_c l_c/2)}{Z_c + Z_{GH} \tanh(\gamma_c l_c/2)}, \quad (2)$$

where Z_c is the characteristic impedance [acoustic shear impedance, $(\rho_c \times c_{66})^{1/2}$], where c_{66} is the shear elastic modulus of the crystal], γ_c is the complex wave propagation factor [$= j\omega(\rho_c/c_{66})^{1/2}$], and l_c is the length of the resonator crystal. Z_{EF} and Z_{GH} represent the acoustic load impedance at the ports EF and GH. The total acoustic impedance (Z_{CD}) at position CD is the parallel arrangement of Z_r and Z_l . Thus, Z_{CD} is

$$Z_{CD} = \frac{1}{\frac{1}{Z_r} + \frac{1}{Z_l}}. \quad (3)$$

The electrical impedance (Z_{AB}) at port AB can be calculated from

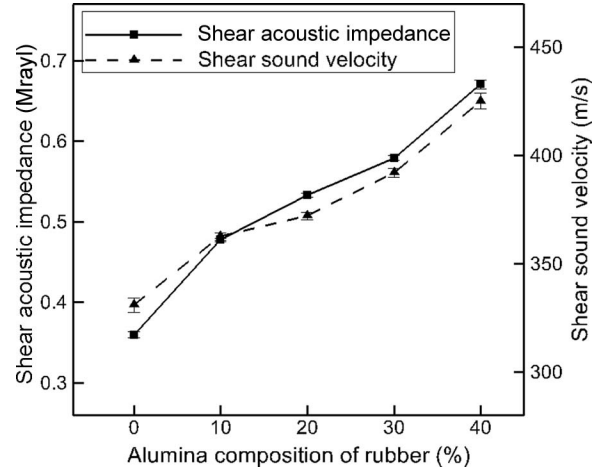


Fig. 4. Shear acoustic impedance and sound velocity of rubber and alumina mixtures.

$$Z_{AB} = \frac{1}{j\omega C_0} + jX_1 + \frac{1}{N^2} Z_{CD}, \quad (4)$$

where

$$jX_1 = \frac{1}{j\omega C_0} \frac{k_{36}^2}{\alpha} \sin \alpha, \quad (5)$$

$$\frac{1}{N^2} = \frac{1}{\omega C_0} \frac{4k_{36}^2}{\alpha} \frac{1}{Z_c} \sin^2 \frac{\alpha}{2}, \quad (6)$$

and

$$\alpha = \omega l_c \sqrt{\frac{\rho_c}{v_c}}. \quad (7)$$

N , X_1 , C_0 , and α represent the turn ratio of the transformer, additional reactance of the equivalent circuit, clamped capacitance of the crystal, and the complex acoustic wave phase shift ($= \pi\omega/\omega_0$), respectively. ρ_c is the crystal density and v_c is the speed of shear sound waves in the crystal. Because the acoustic load (Z_L) was applied to one side of the crystal, we can assume that the load at the port GH (Z_{GH}) is zero and at the port EF (Z_{EF}) is Z_L , as shown in Fig. 1. Finally, the electrical impedance (Z_{AB}) can be obtained for a single-side loaded piezoelectric crystal using (1)–(7) [32]–[36]:

$$Z_{AB} = \frac{1}{j\omega C_0} \left[1 - \frac{k_{36}^2}{\alpha} \frac{2 \tan \frac{\alpha}{2} - j \frac{Z_L}{Z_c}}{1 - j \frac{Z_L}{Z_c} \cot \alpha} \right]. \quad (8)$$

Fig. 3 shows the calculated electrical impedance spectrum of the face-shear-mode resonator with the front load using

TABLE II. INPUT PARAMETERS FOR KLM MODEL.

	l_c (mm)	v_c (m/s)	ρ_c (kg/m ³)	C_0 (nF)	Z_c (Mrayl)	$Z_{L,air}$ (rayl)	$Z_{L,water}$ (Mrayl)
Values	10	1632	8100	2.6	13.2	420	1.5

TABLE III. SPECIFICATIONS OF SINGLE CRYSTAL RESONATORS.

Mode	Crystal	Dimensions (mm)
Thickness (d_{33})	PMN-PT	$10 \times 10 \times 0.5$
Thickness-shear (d_{15})	PMN-PT	$10 \times 10 \times 1$
Face-shear (d_{36})	PIN-PMN-PT	$10 \times 10 \times 1$

the KLM model. At the resonant frequency and anti-resonant frequency, the electrical impedance is changed with different loads such as air and water. Input parameters used for the modeling of face-shear mode resonator are shown in Table II.

IV. EXPERIMENTAL RESULTS AND DISCUSSION

For the acoustic impedance sensing test, we used crystal resonators operating in three different modes, including thickness mode (or d_{33} mode), thickness-shear mode (or d_{15} mode) and face-shear mode (or d_{36} mode). The dimensions of all resonators are listed in Table III. Cr/Au electrodes were sputtered onto 10×10 mm surfaces. For electrical connection to the impedance analyzer, 10-cm co-axial wires (AWG 25, Hitachi Cable Ltd., Tokyo, Japan) were bonded to both electrodes on the resonators using silver epoxy. The silicon rubber (Sylgard 170, Dow Corning Corp., Midland, MI) was used as the carrier material for control of acoustic load variations. Aluminum oxide (Al_2O_3) powders in different percentages by weight were mixed with the liquid silicon rubber. The amount of mixed alumina oxide was 10%, 20%, 30%, and 40% of the silicon rubber by weight. The liquid silicon rubber with or without Al_2O_3 powders was applied to one side of each crystal and cured for 24 h in a vacuum desiccator. The thickness of rubber or rubber/aluminum oxide composite was about 2 mm.

The longitudinal sound velocities of rubber mixtures were measured using the pulse-echo method and then the shear sound velocities were calculated. For pulse-echo tests, the rubber mixture sample was immersed in a water tank and a 30-MHz transducer was located 5 mm away from the top surface of the rubber sample in water. This

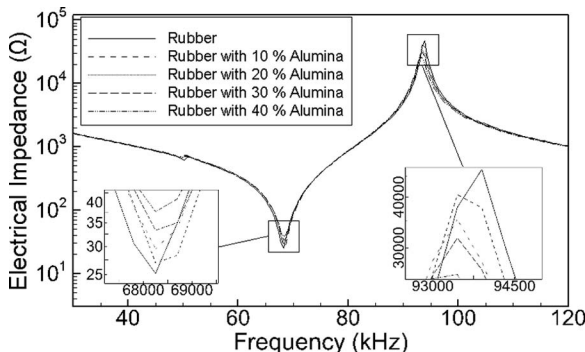


Fig. 5. Measured face-shear-mode resonator behavior with different acoustic load impedances.

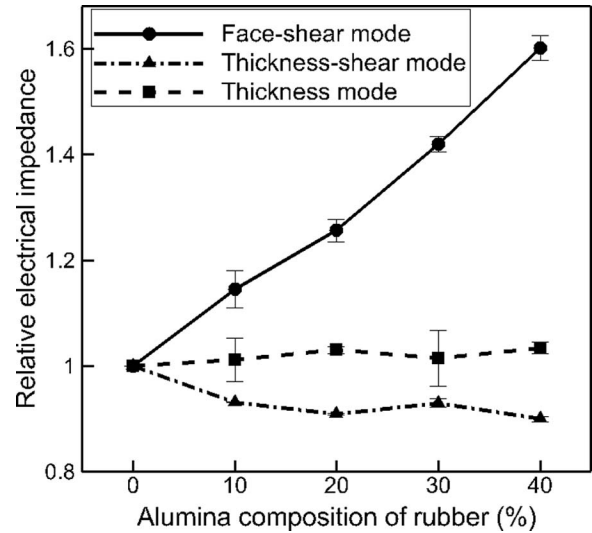


Fig. 6. Relative electrical impedance of each mode at the resonant frequency.

transducer transmitted ultrasound waves into the water and received ultrasound echo signals from the top and bottom surfaces of the rubber targets. The time of flight of pulse-echo waves between the top and bottom surfaces of rubber samples was measured [37]. The shear velocity was calculated from the longitudinal velocity using the Poisson’s ratio of rubbers ($\nu = 0.5$). The dimension and the weight of the rubber mixture were measured using a digital caliper and a micro balance to determine the density of the rubber mixtures. The shear acoustic impedance (Z_s) of rubber mixtures was calculated using

$$Z_s = \rho v_s, \tag{9}$$

where ρ and v_s are the density and the shear sound velocity of the rubber mixtures, respectively. Fig. 4 shows the shear acoustic impedance and shear sound velocity of the

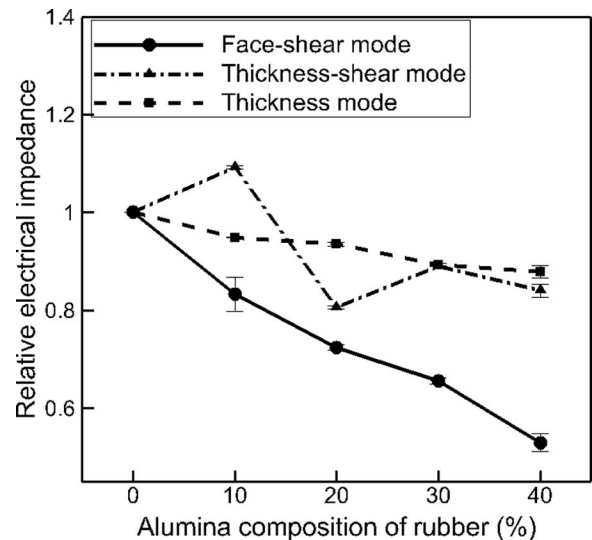


Fig. 7. Relative electrical impedance of each mode at the anti-resonant frequency.

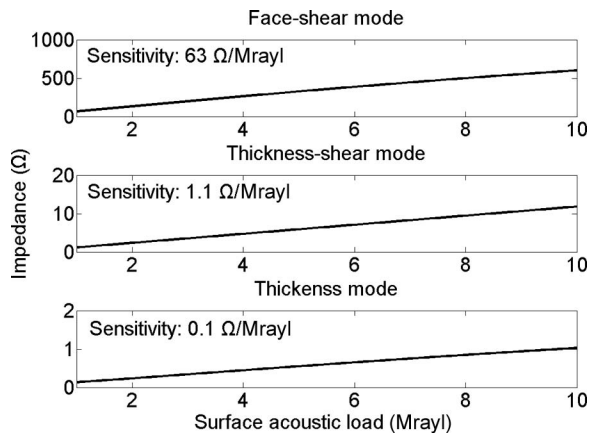


Fig. 8. Calculated sensitivity of face-shear, thickness-shear, and thickness-mode resonators at the resonant frequency under different surface loadings (1 to 10 Mrayl).

rubber mixtures. The acoustic impedance and velocity of the rubber mixtures increased with the composition ratio of aluminum oxide powders. The electrical impedance spectrum of each resonator was measured using an impedance analyzer (HP4294A). Fig. 5 shows the measured electrical impedance of face-shear-mode crystal with different acoustic loads for the frequency range from 30 to 120 kHz. The insets show close-ups of the impedance changing with the application of different acoustic loads. The electrical impedance increased at the resonant frequency, whereas it decreased at the anti-resonant frequency, as the acoustic load impedance increased. To compare the performance of resonators operating in different modes, the electrical impedance of each resonator was normalized by the reference impedance (pure rubber loaded resonator). Figs. 6 and 7 present the relative electrical impedance for each vibration mode at the resonance and anti-resonance, respectively. In the case of thickness-shear mode, it was hard to find the relationship between the surface load and the electrical impedance because the change in electrical impedance was too small and the resonance peak was not clear. The sensitivity (S_z) of electrical impedance to applied surface loads can be calculated by using

$$S_z = \left| \frac{dZ_{AB}}{dZ_L} \right|, \quad (10)$$

where dZ_{AB} is the electrical transmitting impedance and dZ_L is the acoustic load impedance. The sensitivity of face-shear mode, thickness-shear mode, and thickness mode were compared, as shown in Table IV. At the resonance, the sensitivity of face-shear mode was about 20 times higher than that of thickness-shear mode and 85

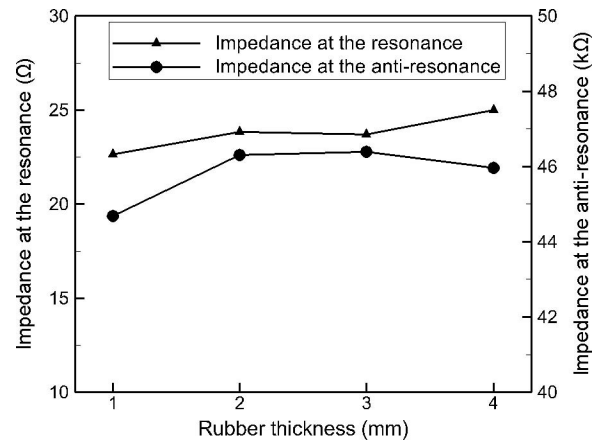


Fig. 9. Electrical impedance of face-shear-mode resonator with different thickness of rubber layers at the resonant and anti-resonant frequencies.

times higher than that of thickness mode. Similarly, at the anti-resonance, face-shear mode showed 95 times and 1400 times higher sensitivity than thickness-shear mode and thickness mode, respectively. As a result, the face-shear-mode resonator was found to be much more sensitive to the surface acoustic loads than its thickness-shear and thickness-mode counterparts at both resonance and anti-resonance. The KLM modeling results for sensitivity of each resonator under different surface loadings are shown in Fig. 8. The calculated sensitivity of the face-shear mode at the resonant frequency was $63 \Omega/\text{Mrayl}$, which was 55 times higher than other modes. The higher mechanical quality factor than other modes, which determines the quality of resonance and the sensitivity to the load, can be the main reason for high sensitivity. These measured sensitivities were slightly lower than the calculated sensitivity values. This was because the wires connected to the resonator could act as an additional resistance and the silver epoxy used for the wire bonding on the resonator surface could be considered as an additional surface load. This unique property of face-shear-mode resonator can be a merit for a broad range of applications such as artificial skins, biological and chemical sensors, touch screens, and other tactile-based sensors which require high sensitivity to the surface load. Fig. 9 shows the impedance of the face-shear resonator with different thickness of rubber layers (1 to 4 mm) at the resonance and anti-resonance. The impedance changes were found to be less than 5%. Because these changes were very small, we assumed that the effect from thickness of rubber was not significant in cases in which the front load thickness is >1 mm. Fig. 10 shows the lateral size effect of the face-shear resonator with different operational frequency. The resonator dimension is

TABLE IV. MEASURED SENSITIVITY OF DIFFERENT MODE CRYSTALS (Ω/Mrayl).

	Face-shear mode	Thickness-shear mode	Thickness mode
Sensitivity at resonance	47	2	0.5
Sensitivity at anti-resonance	74624	785	53

TABLE V. CALCULATED SENSITIVITY AND RESONANT FREQUENCY OF FACE-SHEAR MODE RESONATOR.

Crystal length (mm)	Sensitivity (Ω/Mrayl)	Resonant frequency (kHz)
10	63	68.25
5	126	136.50
2	315	341.25
1	631	682.50

related to the resonator sensitivity because the dimension determines the resonant frequency of the resonator. As the resonant frequency increases, the amount of impedance change—that is, the sensitivity to the surface load—increased. Table V indicates the sensitivity of the face-shear mode resonators with different lateral sizes and resonant frequencies. The sensitivity is inversely proportional to the crystal length, but proportional to the resonant frequency. For example, ideally, the sensitivity of the 1-mm-length resonator was 10 times higher than that of the 10-mm-length resonator. This result supports the idea that miniaturized face-shear resonator arrays are very promising for surface load sensing applications.

V. CONCLUSION

In conclusion, the sensitivity to the acoustic surface load impedance of PIN-PMN-PT resonator was investigated. Different acoustic loads were applied to the thickness-mode, thickness-shear-mode, and face-shear-mode resonators. The highest sensitivity was found from the face-shear-mode resonator, which was found to be about ten times higher than other modes, and which was successfully verified by the KLM model results. It was also found that surface load sensitivity increases with decreased lateral sizes of resonators, which favors large area surface

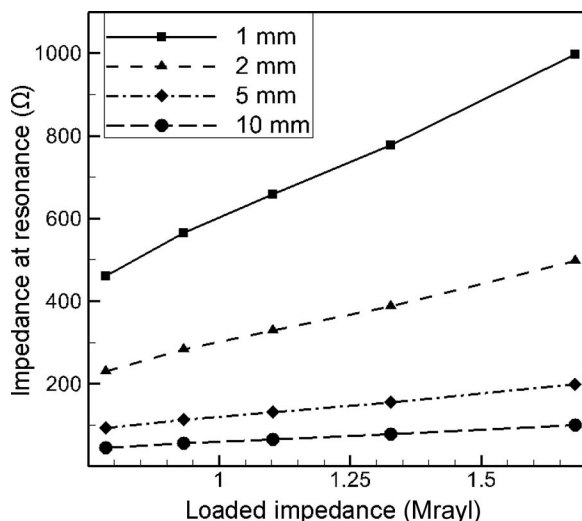


Fig. 10. The size effect of face-shear-mode resonators with lateral sizes from 1 to 10 mm.

sensing using an array of face-shear resonators. The high sensitivity of the face shear mode to the surface load can be promising for applications such as artificial skins, biological sensors, chemical sensors, touch screens, and other tactile-based sensors.

ACKNOWLEDGMENTS

The author thank their lab members, S. Bakshi, L. Tolliver, and S. Guo, for their insightful comments.

REFERENCES

- [1] B. Wickman, H. Grönbeck, P. Hanarp, and B. Kasemo, "Corrosion induced degradation of Pt/C model electrodes measured with electrochemical quartz crystal microbalance," *J. Electrochem. Soc.*, vol. 157, no. 4, pp. B592–B598, 2010.
- [2] X. Wang, B. Ding, J. Yu, M. Wang, and F. Pan, "A highly sensitive humidity sensor based on a nanofibrous membrane coated quartz crystal microbalance," *Nanotechnology*, vol. 21, no. 5, art. no. 055502, 2010.
- [3] V. Jalkanen, B. Andersson, and O. Lindahl, "Stiffness of a small tissue phantom measured by a tactile resonance sensor," in *12th Mediterranean Conf. Medical and Biological Engineering and Computing*, 2010, pp. 395–398.
- [4] T. Hemsell, R. Stroop, D. Oliva Uribe, and J. Wallaschek, "Resonant vibrating sensors for tactile tissue differentiation," *J. Sound Vibrat.*, vol. 308, no. 3–5, pp. 441–446, 2007.
- [5] T. Oie, H. Suzuki, Y. Murayama, T. Fukuda, S. Omata, K. Kanda, K. Takamizawa, and Y. Nakayama, "Surface elasticity imaging of vascular tissues in a liquid environment by a scanning haptic microscope," *J. Artif. Organs*, vol. 13, no. 2, pp. 121–125, 2010.
- [6] Y. Murayama, M. Yoshida, J. Mizuno, H. Nakamura, S. Inoue, Y. Watanabe, K. Akaishi, H. Inui, C. E. Constantinou, and S. Omata, "Elasticity measurement of zona pellucida using a micro tactile sensor to evaluate embryo quality," *J. Mamm. Ova Res*, vol. 25, pp. 8–16, Apr. 2008.
- [7] A. Bonakdar and N. Narayanan, "Determination of tissue properties using microfabricated piezoelectric tactile sensor during minimally invasive surgery," *Sensor Rev.*, vol. 30, no. 3, pp. 233–241, 2010.
- [8] J. Dargahi, R. Sedaghati, H. Singh, and S. Najarian, "Modeling and testing of an endoscopic piezoelectric-based tactile sensor," *Mechatronics*, vol. 17, no. 8, pp. 462–467, 2007.
- [9] C. H. Chuang, "Flexible piezoelectric tactile sensors with structural electrodes array," *Recent Adv. Sens. Technol.*, vol. 49, pt. 6, pp. 189–202, 2009.
- [10] O. Lindahl, C. Constantinou, A. Eklund, Y. Murayama, P. Hallberg, and S. Omata, "Tactile resonance sensors in medicine," *J. Med. Eng. Technol.*, vol. 33, no. 4, pp. 263–273, 2009.
- [11] C. Chuang, "Piezoelectric tactile sensor," U.S. Patent 12828802, Jul. 1, 2010.
- [12] E. Benes, M. Gröschl, W. Burger, and M. Schmid, "Sensors based on piezoelectric resonators," *Sens. Actuators A*, vol. 48, no. 1, pp. 1–21, 1995.
- [13] V. Todorova and D. Kolev, "Design and modeling problems of resonance piezoelectric tactile arrays," in *IEEE Control Applications, (CCA) and Intelligent Control, (ISIC)*, 2009, pp. 1433–1436.
- [14] R. M. Schmitt, W. G. Scott, R. D. Irving, J. Arnold, C. Bardons, D. Halpert, and L. Parker, "Ultrasonic imaging of fingerprints using acoustical impedigraphy," in *IEEE Int. Ultrasonics Symp.*, 2004, pp. 680–688.
- [15] R. M. Schmitt and J. Owen, "Acoustic impedigraphy: Imaging surface acoustic impedance using 1–3 piezo-composite for integrated fingerprinting," in *IEEE 61st Electronic Components and Technology Conf.*, 2011, pp. 1296–1299.
- [16] R. M. Schmitt, "Method and system for multi-mode mechanical resonator," U.S. Patent 12117468, May 8, 2008.
- [17] K. B. Kim, D. K. Hsu, B. Ahn, Y. G. Kim, and D. J. Barnard, "Fabrication and comparison of PMN-PT single crystal, PZT and PZT-based 1-3 composite ultrasonic transducers for NDE applications," *Ultrasonics*, vol. 50, no. 8, pp. 790–797, 2010.

- [18] S. Zhang and F. Li, "High performance ferroelectric relaxor-PbTiO₃ single crystals: Status and perspective," *J. Appl. Phys.*, vol. 111, art. no. 031301, 2012.
- [19] D. Zhou, J. Chen, L. Luo, X. Zhao, and H. Luo, "Optimized orientation of 0.71Pb(Mg_{1/3}Nb_{2/3})O₃-0.29PbTiO₃ single crystal for applications in medical ultrasonic arrays," *Appl. Phys. Lett.*, vol. 93, no. 7, art. no. 073502, 2008.
- [20] K. Rajan, M. Shanthi, W. Chang, J. Jin, and L. Lim, "Dielectric and piezoelectric properties of [0 0 1] and [0 1 1]-poled relaxor ferroelectric PZN-PT and PMN-PT single crystals," *Sens. Actuators A*, vol. 133, no. 1, pp. 110–116, 2007.
- [21] Q. Zhang, J. Zhao, K. Uchino, and J. Zheng, "Change of the weak-field properties of Pb(ZrTi)O₃ piezoceramics with compressive uniaxial stresses and its links to the effect of dopants on the stability of the polarizations in the materials," *J. Mater. Res.*, vol. 12, no. 1, pp. 226–234, 1997.
- [22] J. Luo, W. Hackenberger, S. Zhang, and T. R. Shrout, "Elastic, piezoelectric and dielectric properties of PIN-PMN-PT crystals grown by Bridgman method," in *IEEE Int. Ultrasonics Symp.*, 2008, pp. 261–264.
- [23] Q. F. Zhou, B. P. Zhu, D. W. Wu, C. H. Hu, J. M. Cannata, J. Tian, P. D. Han, and K. K. Shung, "PIN-PMN-PT single crystal high frequency ultrasound transducers for medical applications," in *IEEE Int. Ultrasonics Symp.*, 2008, pp. 1433–1436.
- [24] W. Wang, Y. Zhang, X. Zhao, and H. Luo, "High Curie temperature piezoelectric single crystals Pb(In_{1/2}Nb_{1/2})O₃-Pb(Mg_{1/3}Nb_{2/3})O₃-PbTiO₃ and their applications in medical ultrasonic transducers," in *2010 Symp. Piezoelectricity, Acoustic Waves and Device Applications (SPAWDA)*, pp. 191–195.
- [25] S. Zhang, F. Li, N. P. Sherlock, J. Luo, H. J. Lee, R. Xia, R. J. Meyer Jr., W. Hackenberger, and T. R. Shrout, "Recent developments on high Curie temperature PIN-PMN-PT ferroelectric crystals," *J. Cryst. Growth*, vol. 318, no. 1, pp. 846–850, 2010.
- [26] P. Sun, Q. Zhou, B. Zhu, D. Wu, C. Hu, J. M. Cannata, J. Tian, P. Han, G. Wang, and K. K. Shung, "Design and fabrication of PIN-PMN-PT single-crystal high-frequency ultrasound transducers," *IEEE Trans. Ultrason. Ferroelectr. Freq. Control*, vol. 56, no. 12, pp. 2760–2763, 2009.
- [27] S. Zhang, F. Li, J. Luo, R. Xia, W. Hackenberger, and T. R. Shrout, "Field stability of piezoelectric shear properties in PIN-PMN-PT crystals under large drive field," *IEEE Trans. Ultrason. Ferroelectr. Freq. Control*, vol. 58, no. 2, pp. 274–280, 2011.
- [28] S. Zhang, F. Li, W. Jiang, J. Luo, R. J. Meyer, W. Cao, and T. R. Shrout, "Face shear piezoelectric properties of relaxor-PbTiO₃ single crystals," *Appl. Phys. Lett.*, vol. 98, no. 18, art. no. 182903, 2011.
- [29] R. Bechmann and I. Fair, "IRE standards on piezoelectric crystals: Determination of the elastic, piezoelectric, and dielectric constants—The electromechanical coupling factor," *Proc. IRE*, vol. 46, no. 4, pp. 764–778, 1958.
- [30] S. Zhang, W. Jiang, R. J. Meyer, F. Li, J. Luo, and W. Cao, "Measurements of face shear properties in relaxor-PbTiO₃ single crystals," *J. Appl. Phys.*, vol. 110, no. 6, art. no. 064106, 2011.
- [31] R. Krimholtz, D. Leedom, and G. Matthaei, "New equivalent circuits for elementary piezoelectric transducers," *Electron. Lett.*, vol. 6, no. 13, pp. 398–399, 1970.
- [32] R. W. Cernosek, S. J. Martin, A. R. Hillman, and H. L. Bandey, "Comparison of lumped-element and transmission-line models for thickness-shear-mode quartz resonator sensors," *IEEE Trans. Ultrason. Ferroelectr. Freq. Control*, vol. 45, no. 5, pp. 1399–1407, 1998.
- [33] A. Arnau, Y. Jimenez, and T. Sogorb, "An extended Butterworth Van Dyke model for quartz crystal microbalance applications in viscoelastic fluid media," *IEEE Trans. Ultrason. Ferroelectr. Freq. Control*, vol. 48, no. 5, pp. 1367–1382, 2001.
- [34] R. Lucklum, C. Behling, R. W. Cernosek, and S. J. Martin, "Determination of complex shear modulus with thickness shear mode resonators," *J. Phys. D*, vol. 30, no. 3, pp. 346–356, 1997.
- [35] R. Lucklum and P. Hauptmann, "Determination of polymer shear modulus with quartz crystal resonators," *Faraday Discuss.*, vol. 107, pp. 123–140, 1997.
- [36] C. S. Desilets, J. D. Fraser, and G. S. Kino, "The design of efficient broad-band piezoelectric transducers," *IEEE Trans. Sonics Ultrason.*, vol. 25, no. 3, pp. 115–125, 1978.
- [37] I. Kuo, B. Hete, and K. Shung, "A novel method for the measurement of acoustic speed," *J. Acoust. Soc. Am.*, vol. 88, no. 4, pp. 1679–1682, 1990.



Kyungrim Kim received his B.S. degree in mechanical and automotive engineering from Kookmin University in Korea. In fall 2009, he started his work as a Ph.D. student in the Department of Mechanical and Aerospace Engineering, North Carolina State University. Currently, he is working as a Research Assistant in the Micro/Nano Engineering Laboratory under Dr. Jiang. His main research interests are high-temperature piezoelectric sensors and ultrasonic sensors.



Shujun Zhang received his Ph.D. degree from The State Key Laboratory of Crystal Materials, Shandong University, China, in 2000. He is currently Senior Research Associate at the Material Research Institute and an Associate Professor in the Materials Science and Engineering Department, The Pennsylvania State University. He is an associate editor of the *IEEE Transactions on Ultrasonics, Ferroelectrics, and Frequency Control (UFFC)* and the *Journal of the American Ceramic Society*. He was a recipient of the Ferroelectrics

Young Investigator Award of the IEEE UFFC Society in 2011. He has coauthored more than 200 papers in the area of functional single crystals and ceramics. He is now focusing on the structure–property–performance relationship of high-temperature, high-power, and high-performance piezoelectric crystals and ceramics for sensor and transducer applications.



Xiaoning Jiang received his Ph.D. degree from Tsinghua University in 1997 and postdoctoral training from the Nanyang Technological University and The Pennsylvania State University (1997–2001). He worked in industry (Standard MEMS Inc. and TRS Technologies Inc.) before joining North Carolina State University in 2009 as an Associate Professor of mechanical and aerospace engineering. Dr. Jiang is the author or co-author of two book chapters, one book, more than 10 US patents and patent applications, and more

than 50 technical papers and presentations on piezoelectric composite micromachined ultrasound transducers (PC-MUT), ultrasound for medical imaging and NDE, smart materials and structures, and M/NEMS.